Effect of Operation Parameters on Performance of Tubular Solid Oxide Fuel Cell

Junxi Jia and Renqiu Jiang
College of Power and Energy Engineering, Harbin Engineering University, Harbin, 150001, China

Shengqiang Shen
School of Energy and Power Engineering, Dalian University of Technology, Dalian 116024, China

Abuliti Abudula
Aomori Industrial Research Center, 4-11-6 Daini-tonyacho, Aomori 030-0113, Japan

DOI 10.1002/aic.11372
Published online December 21, 2007 in Wiley InterScience (www.interscience.wiley.com).

A simulation model is developed to analyze steady state and transient operation of a tubular solid oxide fuel cell (SOFC). The performance of the tubular SOFC is compared when the operation parameters such as inlet fuel temperature, inlet oxidant temperature, and inlet oxidant flow rate are changed, respectively. The model includes both electrochemical model and thermal model. The electrochemical model includes the Nernst potential, ohmic polarization, activation polarization, and concentration polarization. The thermal model includes the heat transfer by conduction, convention, and radiation. An analysis is carried out to investigate the effects of the different operation parameters on the hot spot, solid temperature gradient at the steady state, and the response time at the transient state. Numerical results show that the performance of tubular SOFC due to the change of the different operation parameters is different at the steady state. For the transient response such as the same step increase in cell current density, the response time required for the new steady state is different as different operation parameters are changed. © 2007 American Institute of Chemical Engineers *AIChE J,* 54: 554–564, 2008

Keywords: tubular solid oxide fuel cell, electrochemical reaction, heat and mass transfer, simulation

Introduction

A fuel cell is a device that converts the chemical energy into the electricity directly from the reaction of fuel and oxidant. It can achieve greater electrical efficiency than that obtained from conventional heat engine and is also a highly environmentally benign method of electric power production.[1,2]

Planar and tubular geometric configurations are the main designs for solid oxide fuel cells (SOFCs). The tubular has had the longest history, and the technique of designing and manufacturing is relatively mature.[3]

Although there have been some experimental test results on the overall electrochemical performance of tubular SOFCs,[4,5] it is still not enough to guide the design and operation of a SOFC. Computational modeling can be used to investigate the characteristics for the SOFC at various operating conditions, and it is an effective tool for optimization of SOFC and predicting their characteristics at the steady and transient operating states.

Correspondence concerning this article should be addressed to J. Jia at jiajunxi99@sohu.com.

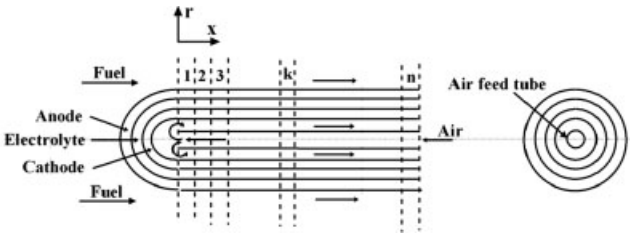

Figure 1. Configuration of tubular SOFC.

There have been many models on the simulation of tubular SOFC at steady and transient state in the open literatures.[3,4,6–20] These models are usually intended for advanced overall system modeling and are a good compromise between accuracy and reasonable computational time.

As we know, not only the current density influences the performance of tubular SOFC as shown in Refs. 3–20, but also other parameters such as inlet fuel temperature, inlet oxidant temperature, and inlet oxidant flow rate could change the characteristics of SOFC. However, the paper that compared and analyzed these operation parameters together is seldom.

Although the hot spot (maximum cell temperature) in the cell components is an important concern for SOFC, it is rather difficult to measure the temperature and find the position of the hot spot. At the same time, the thermal stress of the ceramic cell components is an important criterion for establishing operational limits. During operation, excessive thermal stress may arise due to steep solid temperature gradients. Few of the papers mentioned earlier calculated the position of hot spot and the temperature gradients when the different operation parameters were changed.

Prediction of the transient performance of the fuel cell is important for control purposes. The time required to reach the new steady state should be known in time as the operation parameter changed.

In this study, these steady and transient characteristics of the tubular SOFC were compared when the operation parameters such as inlet fuel temperature, inlet oxidant temperature, and inlet oxidant flow rate were changed, respectively.

Model Description

Cell configuration

Figure 1 shows the configuration of a typical tubular SOFC. Fuel enters the outside of the closed end of the cell. Air is provided inside the cell via an air feed tube and travels to the closed end of the cell. Oxygen in the air fed to the cathode accepts electrons from external circuit to form oxygen ions. The ions are conducted through the solid electrolyte to the anode. At the fuel electrode, the ions combine with hydrogen in the fuel to form water. Electrons flow from the anode through the external circuit back to the cathode. Since the electrochemical reaction is exothermic, the cell produces heat as well as electricity.

Table 1. Geometry Parameters of the Tubular SOFC

Component	Value
Thickness of cathode	2200 μm
Thickness of anode	100 μm
Thickness of electrolyte	40 μm
Thickness of air injection tube	1 mm
Outer diameter of cell	22 mm
Outer diameter of air feed tube	12 mm
Length of Cell	150 cm

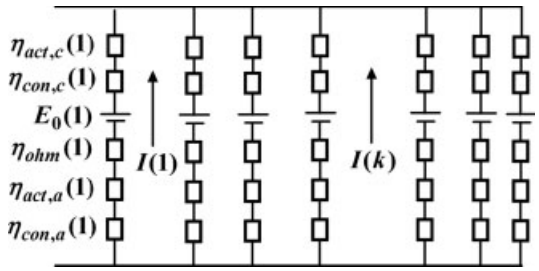

Figure 2. Cell equivalent electric circuit.

The dimensions of the cell and each cell component are listed in Table 1.[21,22]

Electrochemical model

To simulate the electrochemical characteristics of the cell, the tubular cell is divided into slices by the planes perpendicular to x-axis as shown in Figure 1 and is denoted by sliced cell. The driving potential, electrical current, and polarizations are calculated for each slice. A circuit composed of electromotive forces and cell impedances models a sliced cell. Figure 2 shows the cell equivalent electric circuit.

The cell terminal voltage is constant because the electrode materials are good electric conductors and the resistance of Ni felt used for the electrical contact between cells is sufficiently low. However, the driving Nernst potential varies along the cell length. The varying Nernst potential produces varying local current densities. The nonuniform current results in locally varying voltage polarizations. Each local Nernst potential is reduced to the terminal voltage by the sum of the local voltage polarizations. Therefore the cell terminal voltage is given by

$$V = E_0 - \eta_{\mathrm{act,a}} - \eta_{\mathrm{act,c}} - \eta_{\mathrm{ohm}} - \eta_{\mathrm{con,a}} - \eta_{\mathrm{con,c}} \qquad (1)$$

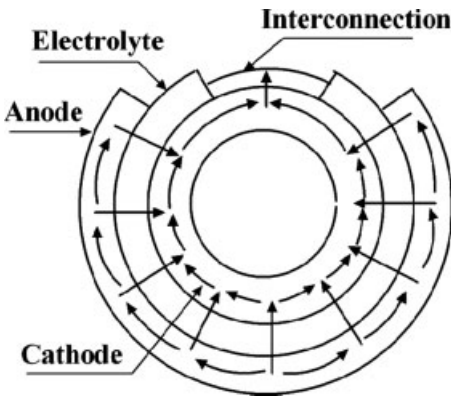

Figure 3. Current path of tubular SOFC.

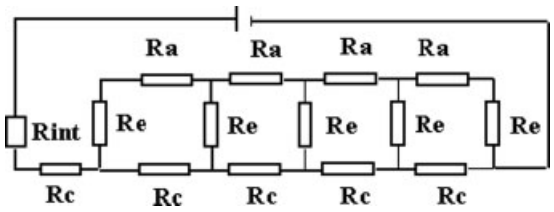

Figure 4. Equivalent electric circuit of the ohmic resistance.

where V is the cell potential and E_0 is the Nernst potential, which is calculated by

$$E_0 = \frac{-\Delta G_0}{2F} + \frac{RT}{2F} \quad \ln \frac{P_{H_2}(P_{O_2})^{1/2}}{P_{H_2O}} \tag{2}$$

Activation Polarization. The development of electrochemical reaction requires overcoming an activation energy barrier. The electrode potential to overcome this activation energy is called the activation polarization. This phenomenon can be described by the Bulter–Volmer equation.[23]

$$i = i_0 \left\{ \exp\left(\frac{\alpha z F \eta_{act}}{RT}\right) - \exp\left[\frac{-(1-\alpha) z F \eta_{act}}{RT}\right] \right\} \tag{3}$$

where α is the transfer coefficient, z is the number of electrons participating in the electrode reaction, F is the Faraday constant, and i_0 is the exchange current density that can be calculated as

$$i_{0,a} = \gamma_a \left(\frac{P_{H_2}}{P_{0,a}}\right)\left(\frac{P_{H_2O}}{P_{0,a}}\right) \quad \exp\left(-\frac{E_{act,a}}{RT}\right) \tag{4}$$

$$i_{0,c} = \gamma_c \left(\frac{P_{O_2}}{P_{0,c}}\right)^{0.25} \quad \exp\left(-\frac{E_{act,c}}{RT}\right) \tag{5}$$

Values for $\gamma_a, \gamma_c, E_{act,a}, E_{act,c}$ could be found in Ref. 23.

Ohmic polarization

Ohmic losses occur because of resistance resulting from the flow of ions in the electrolyte and the flow of electrons through the electrode. Because of the symmetric current flow about the two halves of the cell in Figure 3, it is only necessary to calculate the resistance of a half slice. The total resistance of a cell slice is the parallel combination of the two halves. The equivalent electric circuit of the ohmic resistance for calculation is given in Figure 4.

The cell equivalent ohmic resistance depends on the anode, cathode, and electrolyte resistances.

Table 2. Properties of SOFC Components

	Resistivity (Ωcm)	Pore Radius of Electrode (μm)	τ / ε	Thermal Conduction (W m^{-1} K^{-1})	Emissivity
Cathode	0.008114 exp(600/T)	1	3/30%	9.6	0.9
Electrolyte	0.00294 exp(10350/T)	–	–	2.7	–
Anode	0.00298 exp(−1392/T)	1	3/30%	6.23	–
Air feed tube	–	–	–	6.04	0.9

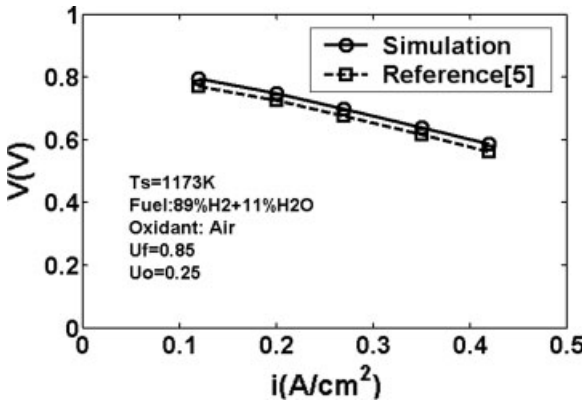

Figure 5. Prediction and experiment results of voltage vs. current density.

Ohmic polarization is expressed by Ohm's law:

$$\eta_{ohm} = I \Sigma R_i \tag{6}$$

where $R_i = \frac{\rho_i \delta_i}{A_i}$ is the ohmic resistance of anode, cathode, and electrolyte in each share of the equivalent circuit of Figure 4, A_i is the respective area of the section where the current flows, δ_i is the corresponding current flow length, and ρ_i is the material resistivity, which is a strong function of temperature as given in Table 2.[1,3]

Concentration polarization

The analysis of concentration polarization should begin with the analysis of the transport of gases through porous electrodes. The electrode concentration overpotential considers the difference in gas concentrations between the electrode–electrolyte interface and the bulk. Mass transport models inside the porous SOFC electrode must be applied to estimate gas concentrations at the electrode–electrolyte interface. In this model, both ordinary and Knudsen diffusions are considered. The model has taken into account the physical properties of SOFC material like porosity, tortuosity, and pore size of the electrode materials. The diffusion polarization is given by two terms, related to the anode and cathode side:

$$\eta_{con} = \frac{RT}{2F} \ln \frac{X^0_{H_2} X^r_{H_2O}}{X^r_{H_2} X^0_{H_2O}} + \frac{RT}{4F} \ln \frac{X^0_{O_2}}{X^r_{O_2}} = \eta_{con,a} + \eta_{con,c} \tag{7}$$

where X^0_i and X^r_i is the molar fraction of specie i in the bulk and at the electrode–electrolyte interface, respectively, which

Table 3. Condition and Parameters for Simulation

Fuel inlet composition (molar fraction)	89%H_2 + 11%H_2O
Oxidant inlet composition (molar fraction)	21%O_2 + 79%N_2
Fuel inlet temperature (K)	1173
Oxidant inlet temperature (K)	1173
Fuel inlet flow rate (mol s^{-1})	1.96×10^{-3}
Oxidant inlet flow rate (mol s^{-1})	3.73×10^{-2}
Operation pressure (atm)	1

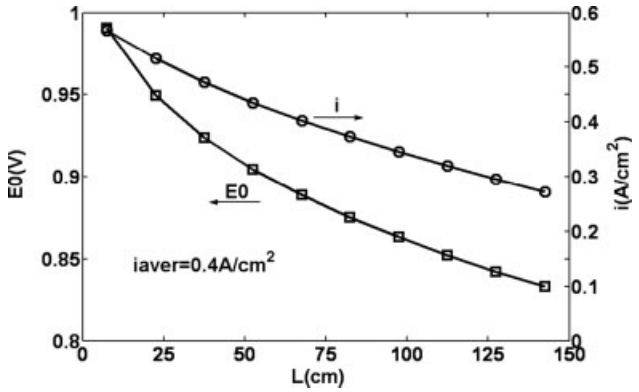

Figure 6. Nernst voltage and current density profiles.

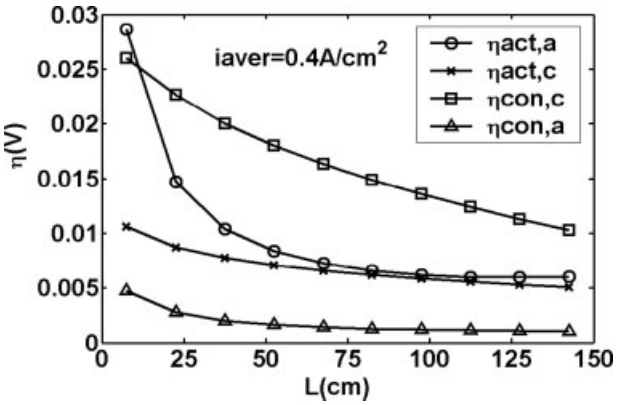

Figure 8. Activation and concentration polarization profiles.

can be estimated by the Fick's law:

$$J_i = -D_{i,}\frac{dC_i}{dr} \tag{8}$$

where $D_i = \left[\frac{\tau}{\varepsilon}\left(\frac{1}{D_{i,m}} + \frac{1}{D_{i,K}}\right)\right]^{-1}$ is the mass diffusion coefficient of specie i in the mixture, $D_{i,K}$ is the Knudsen diffusion coefficient of species i, ε is porosity, and τ is tortuosity.

Applying the Kirchhoff's law of current, the currents in each share of the equivalent circuit can be obtained.[24,25]

Thermal model

Energy Balance Equations in Tubular SOFC. The cell temperatures influence the electrochemical model, and these temperatures affect the local driving voltage, polarizations, and heat generation within the cell. A thermal model has been developed to determine these temperatures by a finite-volume approach. In the electrochemical model, the cell is divided into axial sections or slices. In the thermal model, the same sections are used and each section is composed of the solid structure, air feed tube, and flow passages volumes. Energy balances equations for such volumes in each section can be described as follows.

The general form of the energy conservation equation for a control volume is,

$$\frac{dE_{\text{cv}}}{dt} = \dot{Q}_{\text{CV}} - \dot{W}_{\text{CV}} + \sum_i n_i h_i|_{\text{in}} - \sum_i n_i h_i|_{\text{out}} \tag{9}$$

where E_{CV} is the internal energy (J), $\dot{Q}_{\text{CV}}$ is rate of thermal energy (W) transferred across the control volume, $\dot{W}_{\text{CV}}$ is the rate of work transferred across the control volume, $\sum_i n_i h_i|_{\text{in}}$ is the enthalpy gained due to mass flowing into the element, and $\sum_i n_i h_i|_{\text{out}}$ is the enthalpy loss due to mass flowing out of the element. The mole flow rate of gas species i for fuel and oxidant in the annulus channels can be calculated by means of Faraday's law:

$$n_{\text{H}_2}^{k+1} = n_{\text{H}_2}^{k} - \frac{I_k}{2F} \tag{10}$$

$$n_{\text{H}_2\text{O}}^{k+1} = n_{\text{H}_2\text{O}}^{k} + \frac{I_k}{2F} \tag{11}$$

$$n_{\text{O}_2}^{k+1} = n_{\text{O}_2}^{k} - \frac{I_k}{4F} \tag{12}$$

$$n_{\text{N}_2}^{k+1} = n_{\text{N}_2}^{k} \tag{13}$$

For the steady state, lefthand term in Eq. 9 is eliminated. The change rate of internal energy is given by:

$$\frac{dE_{\text{CV}}}{dt} = \rho\, C_v(\Delta V)\frac{dT}{dt} \tag{14}$$

where ρ is the density (kg m^{-3}), C_{V} is the specific heat at constant volume (J kg^{-1} K^{-1}), ΔV is the elemental volume (m^3), T is the absolute temperature (K), and t is time(s).

Tracking of the energy flows in the cell proceeds by making separate energy balances for the air in the air feed tube, cathode gas, fuel gas, and solid structure.

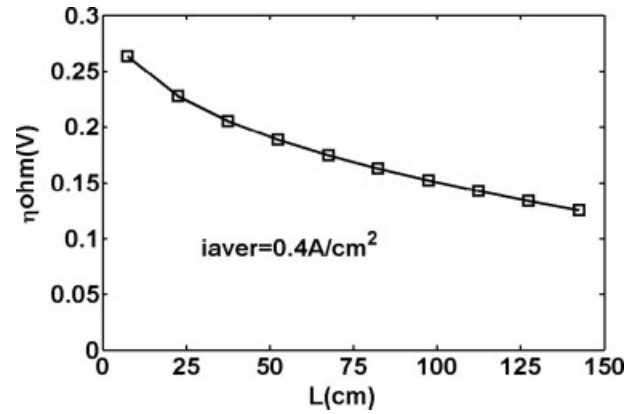

Figure 7. Ohmic polarization profiles.

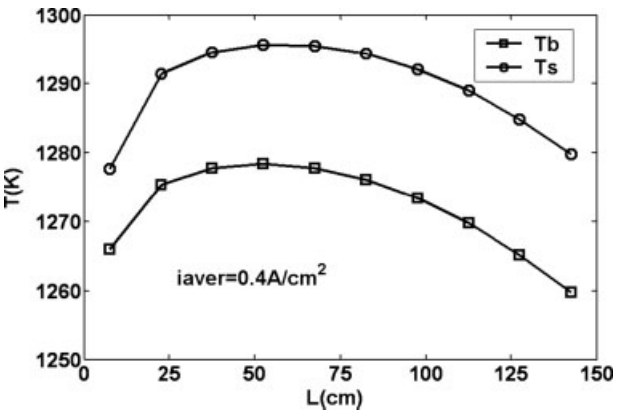

Figure 9. Temperature profiles of solid in the tubular SOFC.

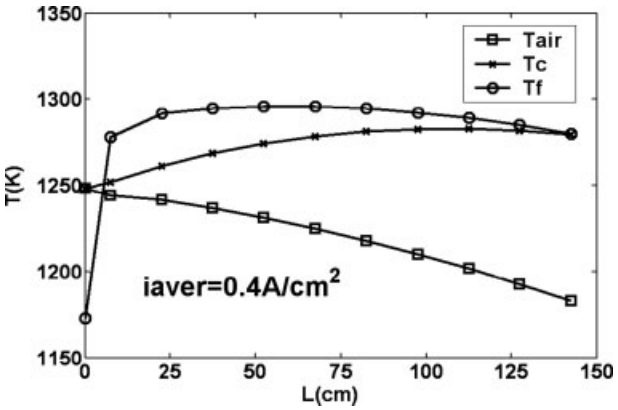

Figure 10. Temperature profiles of gas in the tubular SOFC.

The energy balances for air preheating volume is expressed as:

$$\rho_{\text{air}}\, c_{\text{V}}^{\text{air}} \Delta V_{\text{air}} \frac{T_{\text{air}}^{k,p+1} - T_{\text{air}}^{k,p}}{\Delta t} = \sum_i n_i^{k+1} h_i^{k+1} - \sum_i n_i^k h_i^k + K_{\text{air}} A_{\text{a}} (T_b^k - T_{\text{air}}^k) \quad (15)$$

where K_{air} is the convective heat transfer coefficient between the air preheating and air feed tube and A_{a} is the heat transfer area, p is the time index, and Δt is the change in time from time step p to time $p + 1$. For the full-developed laminar flow,[26] the heat transfer coefficient is expressed by

$$K = Nu \frac{\lambda_{\text{g}}}{D_{\text{e}}} \quad (16)$$

where λ_g is the thermal conductivity of the mixed gas, and D_{e} is the equivalent diameter.

The cathode gas energy balance can be written as,

$$\rho_{\text{c}}\, c_{\text{V}}^{\text{c}} \Delta V_{\text{c}} \frac{T_{\text{c}}^{k,p+1} - T_{\text{c}}^{k,p}}{\Delta t} = \sum_i n_i^{k-1} h_i^{k-1} - \sum_i n_i^k h_i^k + K_{\text{bc}} A_{\text{c}}^{\text{b}} (T_{\text{b}}^k - T_{\text{c}}^k) + K_{\text{sc}} A_{\text{c}}^{\text{s}} (T_{\text{s}}^k - T_{\text{c}}^k) - \frac{I_k}{4F} h_{\text{O}_2}^k \quad (17)$$

where K_{be} is the convective heat transfer coefficient between the cathode gas and air feed tube and K_{SC} is the convective heat transfer coefficient between solid cell and bulk cathode air flow. The last term on the right hand side is the rate of energy accompanying mass transfer of oxygen out of the bulk to the cathode solid.

Table 4. Effect of Average Current Density on Performance of SOFC

	i_{aver} (A/cm^2)		
	0.3	0.4	0.5
V (V)	0.7571	0.6965	0.6404
W (W)	130.3	159.9	183.83
$T_{\text{s,aver}}$ (K)	1256	1289.5	1331.2

The time varying energy conservation equation for fuel gas can be written as,

$$\rho_f\, c_V^f \Delta V_f \frac{T_f^{k,p+1} - T_f^{k,p}}{\Delta t} = \sum_i n_i^{k-1} h_i^{k-1} - \sum_i n_i^k h_i^k + K_{sf} A_f^s (T_s^k - T_f^k) - \frac{I_k}{2F} (h_{\text{H}_2}^k - h_{\text{H}_2\text{O},T_s}^k) \quad (18)$$

where the first and the second term on the right hand side are the rates of energy transfer accompanying the fuel mass flow into and out of the element, the third term is the convective heat flux from the solid cell to the fuel gas, and the last term is the sum of the energy accompanying mass transfer of reactant (H_2) and reaction product (H_2O).

The solid cell unsteady energy balance is written as,

$$\rho_s\, c_V^s \Delta V_s \frac{T_s^{k,p+1} - T_s^{k,p}}{\Delta t} = \frac{\lambda_s}{\delta x} A_{\lambda s} (T_s^{k-1} - T_s^k) - \frac{\lambda_s}{\delta x} A_{\lambda s} (T_s^k - T_s^{k+1}) + K_{sf} A_f^s (T_f^k - T_s^k) + K_{sc} A_c^s (T_c^k - T_s^k) - \frac{A_b \sigma [(T_s^k)^4 - (T_b^k)^4]}{1/\varepsilon_b + \frac{A_b}{A_s}(1/\varepsilon_s - 1)} - \frac{I_k}{2F} \Delta H_{\text{H}_2\text{O},T_s} - W^k \quad (19)$$

where the former five terms on the right of Eq. 19 are the net energy transferred to the cell by heat transfer via conduction, convection, and radiation. The sixth term is the net energy addition by the convective flux of reacting species to the solid cell and subsequent release of their respective reaction enthalpies. The last term is the electrical energy generated in the solid cell due to electrochemical oxidation of hydrogen.

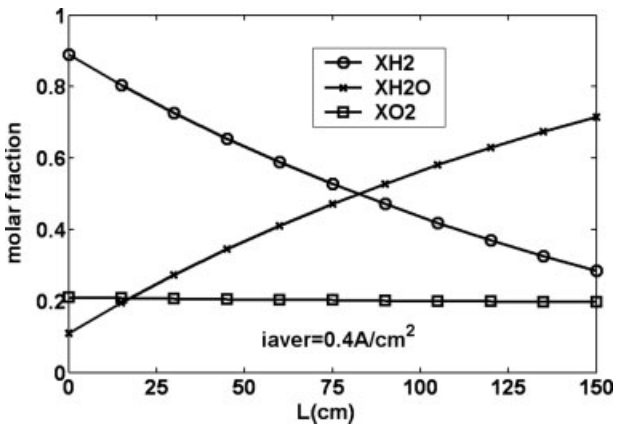

Figure 11. Flow chemical composition profile.

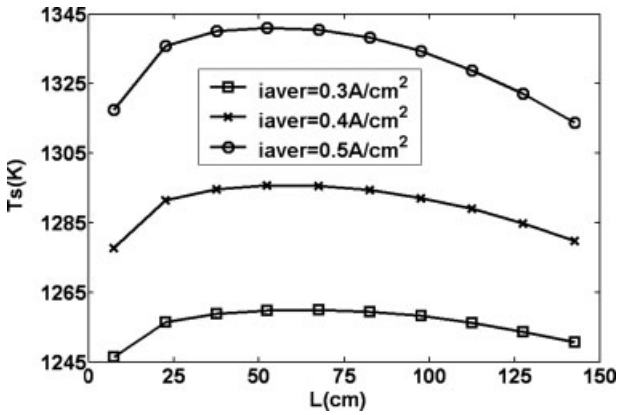

Figure 12. Cell temperature distribution.

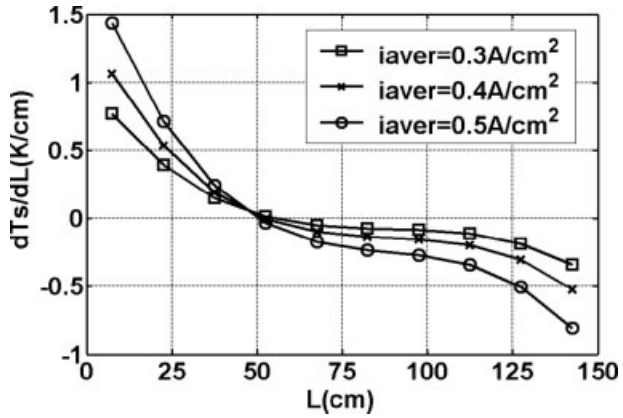

Figure 13. Cell temperature gradient distribution.

The energy balances for air feed tube is expressed as:

$$\rho_b c_V^{\mathrm{b}} \Delta V_b \frac{T_b^{k,p+1} - T_b^{k,p}}{\Delta t} = \frac{\lambda_b}{\delta_x} A_{\lambda b}(T_b^{k-1} - T_b^k) - \frac{\lambda_b}{\delta x} A_{\lambda b}(T_b^k - T_b^{k+1}) + K_{\mathrm{air}} A_a (T_{\mathrm{air}}^k - T_b^k) + K_{bc} A_c^b (T_c^k - T_b^k) + \frac{A_b \sigma[(T_s^k)^4 - (T_b^k)^4]}{1/\varepsilon_b + \frac{A_b}{A_s}(1/\varepsilon_s - 1)} \quad (20)$$

Boundary Conditions. The boundary conditions for the energy conservation equations are as follows.

As the cell is divided into n sections, at the entrance of the air and fuel,

$$T_{\mathrm{air}}^{n+1} = T_{\mathrm{air}}|_{\mathrm{inlet}} \quad (21)$$

$$T_{\mathrm{f}}^0 = T_{\mathrm{f}}|_{\mathrm{inlet}} \quad (22)$$

The air preheating becomes the cathode gas at the exit of the air feed tube, therefore, the continuity between the feed air and the cathode gas can be expressed as,

$$T_{\mathrm{air}}^0 = T_{\mathrm{c}}^0 \quad (23)$$

The outlet end of cell is considered adiabatic, that is, the temperature at the end of the cell is constant.

$$T_{\mathrm{s}}^n = T_{\mathrm{s}}^{n+1} \quad (24)$$

Numerical Solution Algorithm. In a SOFC, current and temperature distributions are strongly coupled. The electrochemical model is solved with a tentative temperature profile. The electrochemical model determines the Nernst potential, current, and electric power. The thermal model accepts these results from electrochemical model and calculates the temperature of the gases and solids. Their temperatures are applied to the electrochemical model for the next calculation of cell Nernst potential, current, and power. As the simulation progressed, the model steps back and forth between electrochemical and thermal calculations until the convergence is obtained. The equations are solved numerically using the Gauss Seidel method.

Results and Discussion

Steady state characteristics

To investigate the accuracy of the model, the calculate *V–I* curve is compared with the test data. Figure 5 shows the numerically predicted cell terminal voltage and the experimental data[5] with different cell current densities. The relative deviation between the calculated voltage and test data is no larger than 5%. Such a good agreement for the terminal voltages between the model-prediction and the experiment shows that the present model is reliable.

The operation conditions and parameters for simulation in the work are listed in Table 3.

When effect of operation parameters on the performance of cell is analyzed respectively, only the studied parameter is changed, all the other input data are assumed as in Table 3.

Effect of Current Density on Steady Performance. Figure 6 shows the local Nernst voltage and current density. Both of them decrease along the *x*-axis. It is because of the fact that along the stream, the depletion of fuel and oxidant has a significant effect on the local Nernst voltage. It is also shown that high Nernst voltage leads to high current density.

The three kinds of polarization losses, which decrease the cell potential from the ideal Nernst value to the real value, are shown in Figures 7 and 8. Among the three polarizations, the ohmic polarization plays the most significant role in the cathode-supported SOFC. The concentration polarization at the anode side is smaller than that at the cathode, because the cathode is thicker than anode and the reactant diffuses through the relatively thick porous cathode to the reaction site at the cathode–electrolyte interface. The concentration polarization at the anode side is negligible with respect to the other losses.

It is important for the SOFC to work under the maximum temperature limit; however, it is difficult to measure the temperature. In the work, the simulated results for the solid temperature profiles along the *x*-axis are shown in Figure 9. Both of the temperature of air feed tube and cell tube increase and then decrease along the *x*-axis, a relatively

Table 5. Effect of Inlet Fuel Temperature on Performance of SOFC

	$T_{\mathrm{f,in}}$ (K)								
	1073*	1123*	1173*	1073†	1123†	1173†	1073‡	1123‡	1173‡
V (V)	0.7542	0.7554	0.7571	0.6940	0.6953	0.6965	0.6389	0.6401	0.6404
W (W)	129.87	130.06	130.3	159.35	159.61	159.9	183.32	183.65	183.83
$T_{\mathrm{s,aver}}$ (K)	1247.5	1250.8	1256.0	1283.2	1286.4	1289.5	1326.6	1329.8	1331.2

*$T_{\mathrm{f,in}}$ calculated for i_{aver} at 0.3 A/cm^2.
†$T_{\mathrm{f,in}}$ calculated for i_{aver} at 0.4 A/cm^2.
‡$T_{\mathrm{f,in}}$ calculated for i_{aver} at 0.5 A/cm^2.

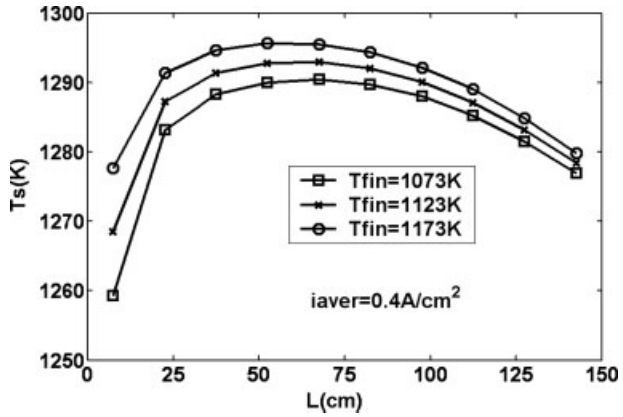

Figure 14. Cell temperature distribution.

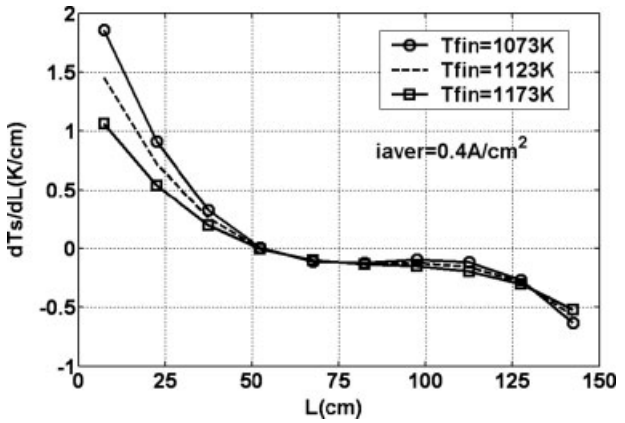

Figure 15. Cell temperature gradient distribution.

higher temperature occurs near the middle part of the cell tube than that at the two ends of the cell tube.

Figure 10 shows the temperature profile for the fuel flow (T_f), the air in the air feed tube (T_{air}), and the cathode gas flow (T_c). The temperatures of air in the feed tube and annulus channel increase gradually in the direction of flow due to the heat transferred by convection. The temperature distribution of fuel is dependent on the temperature of cell tube.

Figure 11 shows the molar fractions variation of gases in the cell along the fuel path. The consumption of the fuel gas and oxidant by electrochemical reaction determines the decrease of hydrogen and oxygen along the x-axis. Hydrogen and oxygen consumption leads to the formation of water vapor. Therefore, the molar fraction of water shows an increase along the x-axis. The excess air is needed to provide air-cooling in SOFC as the allowable temperature rise of the solid cell is limited by the thermal stress induced in the ceramic cell components. Therefore, the change of O_2 molar fraction is not as large as those of H_2 and H_2O.

The overall performance of the tubular SOFC for a series of current densities is given in Table 4. It is clearly shown that high current density leads to high electric power and high average cell temperature.

The cell tube temperature and temperature gradient distribution for three current densities are given in Figures 12 and 13. It indicated that increasing the average current density results in a high cell temperature and temperature gradient distribution. Because the maximum temperature gradient occurs at the two ends of the cell, it can be concluded that the thermal stress problem will most probably occur at the two ends of the cell tube. The hot spot (maximum cell temperature) occurs at the position of 50 cm on the right of the close end of the cell despite the change of the current density. The temperature gradient at the close end of the cell is larger than that at the open end. That is, the thermal stress problem at the close end is more serious than that at the open end of the cell.

Effect of Inlet Fuel Temperature on Steady Performance. An overall performance of the tubular SOFC for different inlet fuel temperatures with a series of current densities is given in Table 5. It can be concluded that increasing the inlet fuel temperature increases the average cell tube temperature. Although the terminal voltage and cell power also increases due to the increase of the inlet fuel temperature, the degree of variation can be ignored.

The cell tube temperature and temperature gradient distribution for three inlet fuel temperatures are given in Figures 14 and 15.

Because the close end of the cell tube receives an impingement of fuel outside of it directly, a high inlet fuel temperature leads to high temperature and more even temperature gradient distribution of the cell tube near the close end.

The hot spot is still near the position of 50 cm on the right of the close end for the different inlet fuel temperatures in this work.

The temperature gradient at the close end of the cell is still larger than that at the open end.

Effect of Inlet Oxidant Temperature on Steady Performance. Table 6 shows the variation of cell terminal voltage and power with current densities for three inlet oxidant temperature cases. The high inlet oxidant temperature leads to an obvious increase of the terminal voltage, power, and average cell tube temperature.

For the same current density, the high inlet oxidant temperature leads to a high cell temperature and temperature

Table 6. Effect of Inlet Oxidant Temperature on Performance of SOFC

	$T_{air,in}$(K)								
	1073*	1123*	1173*	1073†	1123†	1173†	1073‡	1123‡	1173‡
V (V)	0.7135	0.7395	0.7571	0.6533	0.6794	0.6965	0.6022	0.6249	0.6404
W (W)	122.85	127.32	130.3	149.97	155.95	159.9	172.80	179.32	183.83
$T_{s,aver}$ (K)	1166.4	1209.5	1256	1206.4	1248.2	1289.5	1249.9	1289.5	1331.2

*$T_{air,in}$ calculated for i_{aver} at 0.3 A/cm^2.
†$T_{air,in}$ calculated for i_{aver} at 0.4 A/cm^2.
‡$T_{air,in}$ calculated for i_{aver} at 0.5 A/cm^2.

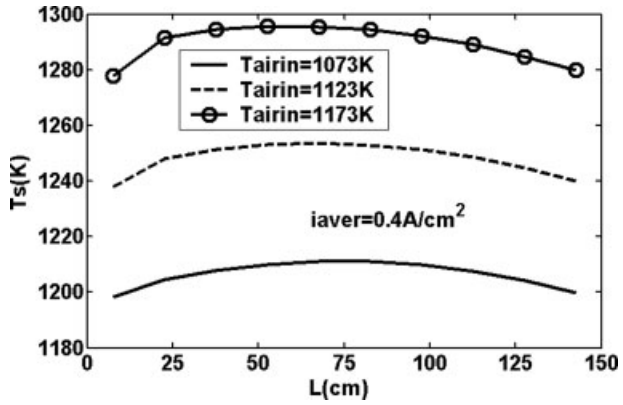

Figure 16. Cell temperature distribution.

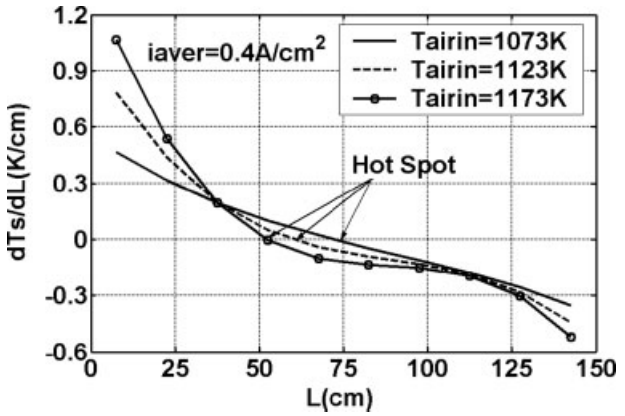

Figure 17. Cell temperature gradient distribution.

gradient distribution at the two ends of the tube as shown in Figures 16 and 17.

The position of the hot spot, that is, the maximum temperature of the tube, in Figure 17 varies significantly with the difference of the inlet oxidant temperature. At a low inlet oxidant temperature, a hot spot occurs in the middle of the cell, with an increase of the temperature, the hot spot moves to the close end of the cell tube by 25 cm. And the higher temperature of the inlet oxidant leads to the larger temperature gradient of the cell at the two ends of cell. At the same time, the temperature gradient at the close end of the cell is larger than that at the open end.

Effect of Oxidant Flow Rate on Steady Performance. The increase of the oxidant flow rate leads to a slight decrease of the terminal voltage and power as given in Table 7, 100% flow rate of the oxidant is defined as in Table 3.

For the same current density, the effect of oxidant flow rate on the cell tube temperature and temperature gradient distribution are given in Figures 18 and 19.

The excess air is needed to provide air-cooling in SOFC, as the allowable temperature rise of the solid cell is limited by the thermal stress induced in the ceramic cell components.

Figures 18 and 19 show that although the temperature gradient at the close end of the cell is still larger than that at the open end, high excess air reduces both the overall cell temperature and temperature gradient and makes the cell temperature more uniform.

Transient simulation

Prediction of the transient performance of the fuel cell is important for control purposes. An investigation of the tubular SOFC transient behavior is studied. In general, the external load can be either load current or load voltage. In this study, we use external step current change and analyze the cell overall transient response. The inlet gas compositions and inlet temperatures of fuel and oxidant are kept constant as shown in Table 3 in this simulation.

First, the increased current of +67% from 0.3 to 0.5 A cm^{-2} is used in the transient simulation.

As shown in Figure 20, the minimum voltage during this load change is 061 V. At the new steady state condition, the voltage reaches a final value of 0.64 V.

Figure 21 shows the transient temperature profiles of the cell and Figure 22 shows the minimum, average, and maximum temperature during the load change. The maximum temperature increases from 1260 K up to 1341.3 K. The maximum, minimum, and average temperatures show a decaying type of growth toward their final values. The transient response time from the old steady state to the new one is 1215 s. These curves show the same trends as those presented in Refs. 27, 28 for the planar stack.

If the current increases by +25% from 0.4 to 0.5 A cm^{-2}, the response time will be 1017 s, shorter than that from 0.3 to 0.5 A cm^{-2}. The contrasted figure of voltage is shown in Figure 23.

To investigate the effect of the inlet fuel temperature, inlet oxidant temperature, and inlet oxidant flow rate on the transient performance of the tubular SOFC, the transient response has been simulated as the average current density step increases from 0.4 to 0.5 A cm^{-2} at $t = 0$ s. During the simulation, only the studied parameter is changed, all the other parameters are assumed as in Table 3.

Table 7. Effect of Inlet Oxidant Flow Rate on Performance of SOFC

	Oxidant Flow rate								
	80%*	100%*	120%*	80%†	100%†	120%†	80%‡	100%‡	120%‡
V (V)	0.7612	0.7571	0.7532	0.7041	0.6965	0.6911	0.6475	0.6404	0.6335
W (W)	131.05	130.3	129.63	161.65	159.9	158.68	185.81	183.83	181.78
$T_{s,aver}$ (K)	1272.5	1256	1242.9	1317.6	1289.5	1274.1	1360.4	1331.2	1309.3

*Oxidant Flow rate calculated for i_{aver} at 0.3 A/cm^2.
†Oxidant Flow rate calculated for i_{aver} at 0.4 A/cm^2.
‡Oxidant Flow rate calculated for i_{aver} at 0.5 A/cm^2.

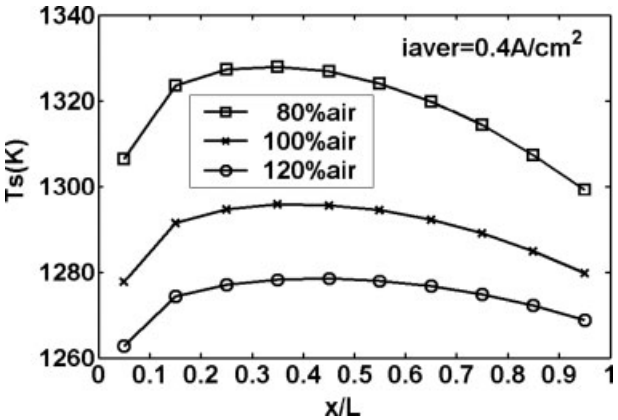

Figure 18. Cell temperature distribution.

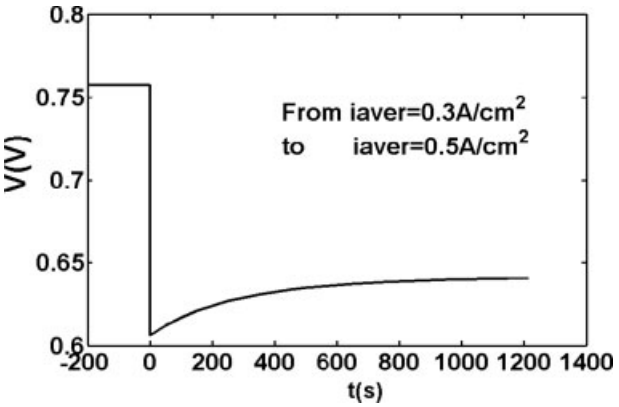

Figure 20. Terminal voltage response due to current step increase.

For the same step increase in current density from 0.4 to 0.5 A cm^{-2}, the effect of the inlet fuel temperature on the transient electrical response is shown in Figure 24. For the inlet fuel temperature of 1123 and 1173 K, the time to reach the final steady state is 1390 and 1017 s, respectively.

It is obvious that higher the inlet fuel temperature, the quicker the tubular SOFC gets to the final steady state.

The effect of the inlet oxidant temperature on the .transient electrical response is shown in Figure 25. For the inlet oxidant temperature of 1123 and 1173 K, the response time is 1129 and 1017 s, respectively. It is shown that a high inlet oxidant temperature leads to the quick response to load change. Although increasing inlet fuel and oxidant temperature by 50 K respectively could short the response time and increase the electric power, it is obvious that the latter leads to evident change in cell power in the short interval.

The effect of the inlet oxidant flow rate on the transient electrical response is shown in Figure 26. For the inlet oxidant flow rate of 80 and 100%, the response time is respectively 717 and 1017 s. The former results in the shorter response time from the initial steady state to the final steady state.

Conclusions

A model has been developed to simulate the steady and transient characteristics of a tubular SOFC. The performance of the tubular SOFC is compared when the operation parameters such as inlet fuel temperature, inlet oxidant temperature, and inlet oxidant flow rate were changed, respectively.

It is found that ohmic loss is the biggest one among the three polarizations in the cathode-supported SOFC. A relatively higher temperature occurs near the middle part of the SOFC than that at two ends of fuel cell, whereas temperature gradient is more obvious at the two ends of the cell, which lead to larger thermal stresses. And in this work, the temperature gradient at the close end of the cell is larger than that at the open end.

A higher inlet fuel temperature results in a little change of the voltage and power and more even temperature gradient distribution of the cell tube near the close end. Both the lower inlet oxidant temperature and higher excess air could decrease the voltage and power and lead to temperature gradient more even at the two ends of the cell.

The transient electrical response and the change in temperature profile were simulated. For the same load change, the response time is shorter at the smaller oxidant flow rate. Increasing the temperatures of the inlet oxidant and fuel

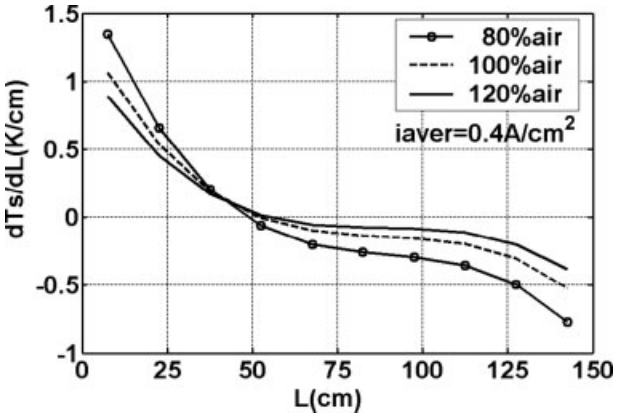

Figure 19. Cell temperature gradient distribution.

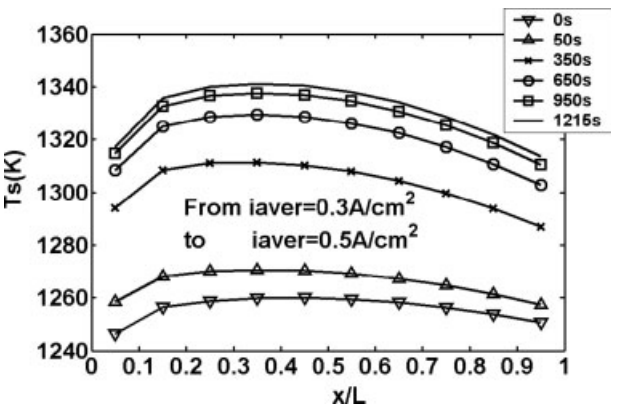

Figure 21. Cell temperature distribution.

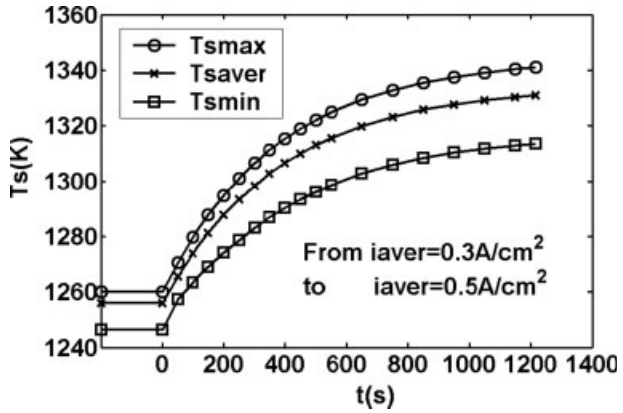

Figure 22. Max, min, and average temperature distribution of the solid structure.

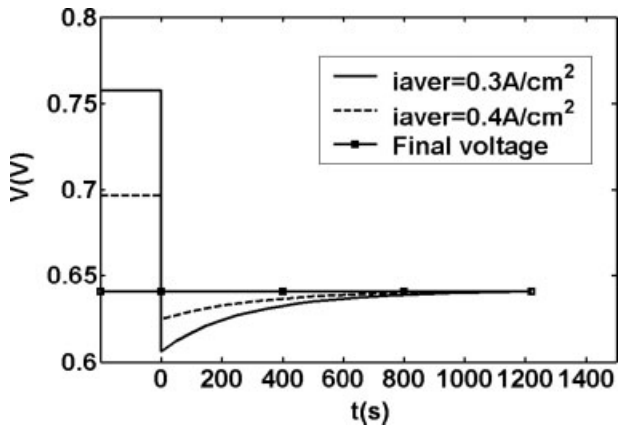

Figure 23. Effect of step increase in current density on the terminal voltage transient response.

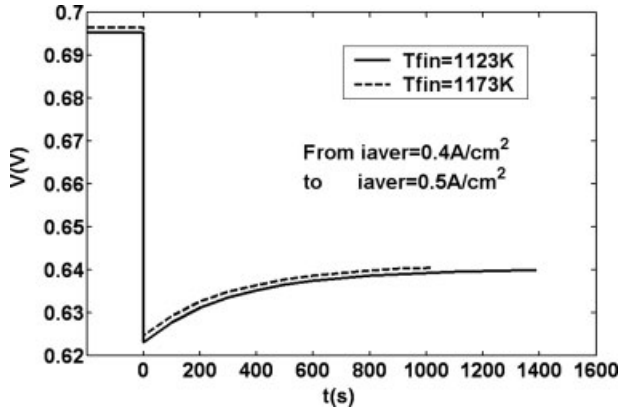

Figure 24. Effect of the inlet fuel temperature on the terminal voltage transient response.

respectively leads to the quicker response of cell from the initial steady state to the final one, whereas the former could adjust the cell to work in wider operation range in shorter interval.

This model and the simulation results can be readily used in tubular SOFC optimization and dynamic control.

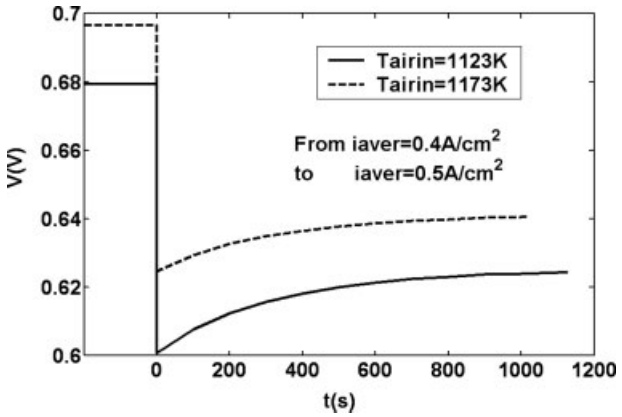

Figure 25. Effect of the inlet oxidant temperature on the terminal voltage transient response.

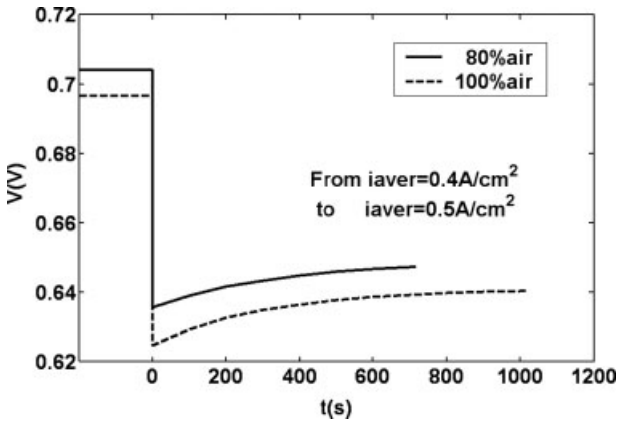

Figure 26. Effect of the flow rate of inlet oxidant on the terminal voltage transient response.

Notation

A = area [m^2]
C = concentration [mol m^{-3}]
C_V = specific heat at constant volume [J kg^{-1} K^{-1}]
ΔV = the elemental volume [m^3]
ΔG = change in Gibbs free energy [J mol^{-1}]
D = diffusion coefficient [m^2 s^{-1}]
E_{act} = activation energy [J mol^{-1}]
F = Faraday constant [96485 C mol^{-1}]
h_i = enthalpy per mole of species i [J mol^{-1}]
ΔH = enthalpy change of the overall reaction [J mol^{-1}]
i = current density [A cm^{-2}]
i_0 = exchange current density [A m^{-2}]
I = current [A]
J_i = transport rate of specie i [mol m^{-2} s^{-1}]
K = heat exchange coefficient [W m^{-2} K^{-1}]
L = length of cell [cm]
n = mole flow rate of gas species i
Nu = Nusselt number
p = partial pressure [atm]
Q = rate of thermal energy transferred across the control volume [W]
r = cell radius coordinate [m]
R = universal gas constant [8.314 J mol^{-1} K^{-1}]
t = time [s]
T = absolute temperature [K]
V = terminal voltage [V]
U_f = fuel utilization
U_o = oxidant utilization

W = electrical power [W]
x = cell axial coordinate [m]
X_i = molar fraction of specie i
z = electrons transferred per reaction

Greek letters

α = transfer coefficient
ε = porosity or emissivity
δ = thickness of cell component [cm]
η = polarization [V]
ρ = specific resistivity [Ω cm]
τ = tortuosity
λ = thermal conductivity of the gas [W m^{-1} k^{-1}]

Subscripts

a = anode
air = air in the air feed tube
act = activation polarization
b = air feed tube
c = cathode
con = concentration polarization
e = electrolyte
f = fuel
ohm = ohm polarization
s = cell solid structure

Literature Cited

1. Massardo AF, Lubelli F. Internal reforming solid oxide fuel cell-gas turbine combined cycles. *J Eng Gas Turbine Power*. 2000;122:27–35.
2. Costamagna P, Magistri L, Massardo AF. Design and part-load performance of a hybrid system based on a solid oxide fuel reactor and a micro gas turbine. *J Power Sources*. 2001;96:352–368.
3. Norman F, Bessette II, Wepfer WJ, Winnick J. A mathematical model of a solid oxide fuel cell. *J Electrochem Soc*. 1995;142:3792–3800.
4. Hirano A, Suzuki M, Lppommatsu M. Evaluation of new solid oxide fuel cell system by non-isothermal modeling. *J Electrochem Soc*. 1992;139:2744–2751.
5. Singhal SC. Advances in solid oxide fuel cell technology. *Solid State Ionics*. 2000;135:305–313.
6. Nagata S, Momma A, Kato T. Numerical analysis of output characteristics of tubular SOFC with internal reform. *J Power Sources*. 2001;101:60–71.
7. Aguiar P, Chadwick D, Kershenbaum L. Modeling of an indirect internal reforming solid oxide fuel cell. *Chem Eng Sci*. 2002;57:1665–1677.
8. Campanari S, Iora P. Definition and sensitivity analysis of a finite volume SOFC model for a tubular cell geometry. *J Power Sources*. 2004;132:113–126.
9. Li P-W, Chyu MK. Simulation of the chemical/electrochemical reactions and heat/mass transfer for a tubular SOFC in a stack. *J Power Sources*. 2003;124:487–498.
10. Li P-W, Schaefer L, Chyu MK. A numerical model coupling the heat and gas species' transport processes in a tubular SOFC. *J Heat Transfer*. 2004;126:219–229.
11. Songa TW, Sohna JL, Kimb JH, Kimc TS, Roa ST, Suzukid K. Performance analysis of a tubular solid oxide fuel cell/micro gas turbine hybrid power system based on a quasi-two dimensional model. *J Power Sources*. 2005;142:30–42.
12. Suwanwarangkul R, Croiset E, Pritzker MD, Fowler MW, Douglas PL, Entchev E. Mechanistic modelling of a cathode-supported tubular solid oxide fuel cell. *J Power Sources*. 2006;154:74–85.
13. Hall DJ, Colclaser RG. Transient modeling and simulation of tubular solid oxide fuel cell. *IEEE Trans Energ Convers*. 1999;14:749–753.
14. Ota T. Object-based modeling of SOFC system: dynamic behavior of micro-tube SOFC. *J Power Sources*. 2003;118:430–439.
15. Jun-Xi J, Sheng-Qiang S. Evaluation and model of performance of a tubular solid oxide fuel cell. *Chem Res Chin Univ*. 2005;21:577–582.
16. Aguiar P, Adjiman CS, Brandon NP. Anode-supported intermediate-temperature direct internal reforming solid oxide fuel cell. II. Model-based dynamic performance and control. *J Power Sources*. 2005;147:136–147.
17. Nehter P. Two-dimensional transient model of a cascaded micro-tubular solid oxide fuel cell fed with methane. *J Power Sources*. 2006;157:325–334.
18. Padulles J, Ault GW, McDonald JR. An integrated SOFC plant dynamic model for power system simulation. *J Power Sources*. 2000;86:495–500.
19. Sedghisigarchi K, Feliachi A. Dynamic and transient analysis of power distribution systems with fuel cells. I. Fuel-cell dynamic model. *IEEE Trans Energ Convers*. 2004;19:423–428.
20. Xue X, Tang J, Sammes N, Du Y. Dynamic modeling of single tubular SOFC combining heat/mass transfer and electrochemical reaction effects. *J Power Sources*. 2005;142:211–222.
21. George RA, Bessette NF. Reducing the manufacturing cost of tubular SOFC technology. *J Power Sources*. 1998;71:131–137.
22. Hirsochenhofer JH, Stauffer DB, Engelmen RR, Klett MG. *Fuel Cell Handbook*, *5th ed*. Morgantown, West Virginia: U.S. Department of Energy, Office of Fossil Energy, 2000.
23. Costamagna P, Honnegger K. Modeling of solid oxide heat exchanger integrated stacks and simulation at high fuel utilization. *J Electrochem Soc*. 1998;145:3995–4007.
24. Junxi J, Shengqiang S, Xiaohua L, Abuliti A. Analysis of the ohmic polarization in tubular solid oxide fuel cell. *Acta Energiae Solaris Sinica*. 2004;25:457–461.
25. Junxi J, Shengqiang S, Riffat SB, Gillott M. Structural parameters study of a tubular solid oxide fuel cell. *J Energ Inst*. 2005;78:76–80.
26. Keys WM, Crawford ME. *Convective Heat and Mass Transfer*, *2nd ed*. New York: McGraw-Hill, 1980.
27. Achenbach E. Three-dimensional and time-dependent simulation of a planar solid oxide fuel cell stack. *J Power Sources*. 1994;49:333–348.
28. Achenbach E. Response of a solid oxide fuel cell to load change. *J Power Sources*. 1995;57:105–109.

Manuscript received Nov. 13, 2007, revision received Apr. 27, 2007, and final revision received Oct. 19, 2007.